Carbon monoxide gas sensing features of zinc oxide nanoneedles: practical selectivity and long-term stability

Ali Jamshidi Bandari[1] · Shahruz Nasirian[1,2]

Abstract

Zinc oxide (ZnO) as a highly sensitive metal oxide semiconductor is exerting a growing significant influence on the detection of hazardous gases such as carbon monoxide gas (CO). However, elevated operating temperature and humidity have been exhibited the bottleneck of CO detection at ambient conditions. Therefore, in the present work, one-dimensional ZnO nanoneedles (ZON) were synthesized by a simple hydrothermal method, and their resistance-type gas sensor was made and applied for the CO sensing features investigation at environmental conditions. The ZON characterization has exhibited a hexagonal wurtzite phase of the pure crystallized ZnO with porous architecture. The CO sensing properties of the ZON sensor (ZS) were studied in various gas concentrations and relative humidity (RH), to examine these main factors at room temperature. Our handmade sensor was exhibited an appropriate response, long-term stability for more than 4 months, and it had good selectivity to CO concentration than that other gases. Moreover, the ZS showed a linear relationship between the response and not only the gas concentrations at various RHs but also the RH toward different gas concentrations, which is very important for the calibration and practical use. Finally, the CO sensing mechanism of the ZS at ambient conditions was discussed as well.

1 Introduction

At present, hazardous atmospheric pollutions and their noxious effects on human life have become a critical problem for quality civilization. To detect and control of atmospheric gas pollutants, primarily attributed to automobile exhaust and factory emission, gas sensors have been widely developed. Resistance-type gas sensors based on metal oxide semiconductors, due to sensitivity to most gases, excellent selectivity, good portability, low cost, and simple fabrication techniques have attracted great attention between several types of the gas sensors for the quantitative monitoring and detection of different toxic gases [1–6]. Among various metal oxide semiconductors (SMOs), typical n-type Zinc oxide (ZnO) with merit features such as wide direct band gap of

3.37 eV, good morphology properties, high electron mobility, low production cost, excellent chemical properties and appropriate response toward gaseous species such as carbon monoxide gas (CO), is widely used in the resistance-type CO gas sensors [1–4, 7–14]. CO is a colorless, odorless and very toxic pollutant gas, which through respiration being quickly absorbed into the whole body's lungs and bloodstream where it can be easily reacted with hemoglobin (approximately 200 times more than of oxygen) to lose the ability to carry oxygen to organs and tissues. The result is some acute toxic symptoms such as respiratory infection, asthma, nausea, dizziness, and loss of muscular control or even death of tissues [4, 5, 15–17]. Therefore, CO is notorious as an invisible silent killer, so that exposure to 5000 ppm of CO for 10 min is lethal to human [5, 17]. Accordingly, accurate detection and monitoring of CO gas with a simple method at ambient conditions is necessary. In spite the fact that the pure ZnO or its composites with other SMOs or metal ions, have been used extensively as active sensing material in the CO resistance-type gas sensors [1–6, 8, 9, 15–21], the main drawbacks associated with the most of them is their unsatisfied and high typical working temperature (> 100 °C) with the great energy consumption and also low life-time [5–8, 16, 18–22].

✉ Shahruz Nasirian
shahruznasirian@ustmb.ac.ir; shahruznasirian@gmail.com

[1] Department of Electrical and Medical Engineering, College of Electrical and Computer Engineering, Mazandaran University of Science and Technology, Babol, Iran

[2] Department of Basic Sciences, Mazandaran University of Science and Technology, Sardaran 12 Avenue, Sheikh Tabarsi Street, P.O. Box 734, Babol, Iran

It is well known that the realization of new defined one-dimensional morphological structure of ZnO with a high density of surface reaction sites and porosity, is the popular strategy to not only overcome the restrictions of the CO gas sensor operating temperature, but also serve as gas sensor with rapid CO gas response and long-term stability at ambient conditions [2, 4, 6, 16, 18, 23]. However, humidity poses another great challenge in the resistance-type CO gas sensor based on ZnO nanostructure at ambient conditions, because a sensor working with fast response and recovery finds irreparable disorder in situations where the humidity value may change dynamically at room operating temperature [1–4, 15, 24]. Hence, the humidity effect on CO gas sensing of ZnO sensor needs to be more discovered. There is, to the best of our knowledge, very few reports for CO gas sensors based on one-dimensional ZnO nanostructures such as nanoneedle at various humidity conditions and room temperature. Accordingly, we have synthesized ZnO nanoneedles via a facile, simple and low-temperature hydrothermal method, and investigated their CO gas sensing features under different gas concentrations and various relative humidity conditions at room temperature.
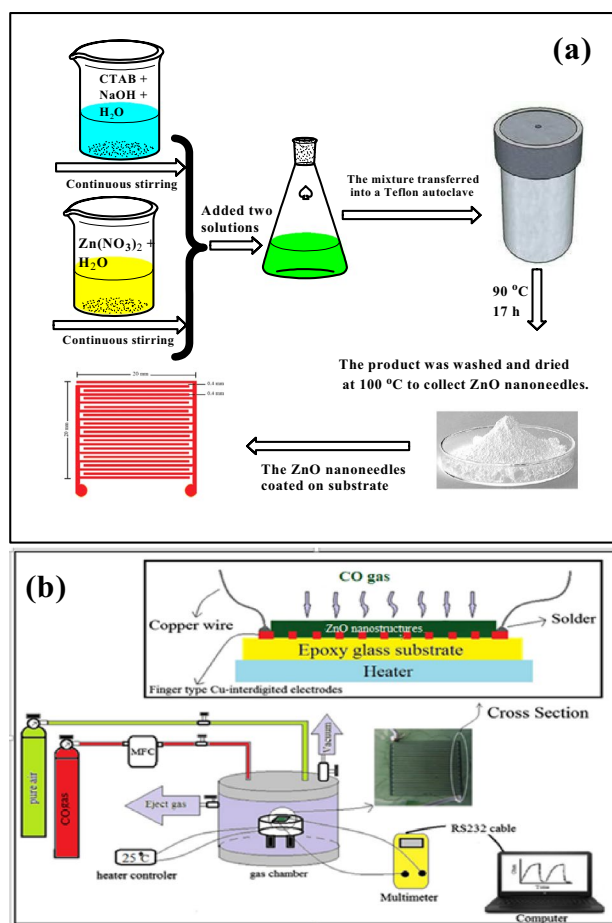
2 Experimental

2.1 Materials

Zinc nitrate hexahydrate ($Zn(NO_3)_2 \cdot 6H_2O$-99% purity), Sodium hydroxide (NaOH-98% purity), Cetyltrimethylammonium bromide (CTAB, $C_{19}H_{42}BrN$-99% purity), Ethanol (99.8% purity) and Polyvinyl alcohol (($C_2H_4O)_x$) were purchased from Merck Co. (Darmstadt, Germany).

2.2 Methods

2.2.1 Synthesis of ZnO nanoneedles

A low-temperature hydrothermal method was used for the synthesis of the ZnO nanoneedles as shown in Fig. 1a. In this typical procedure, 0.3 gr of CTAB with 5.7 gr of NaOH were added into 80 ml of distilled water under stirring [solution (A)]. The solution (B) was created through the adding of $Zn(NO_3)_2 \cdot 6H_2O$ (2.34 gr) into 20 ml of distilled water under continuous stirring. Then, the solution (B) was dropwise added to the solution (A) under stirring at room temperature. The product mixture was transferred into a Teflon autoclave (150 ml), sealed and heated at 90 °C for 17 h in an oven. Consequently, the autoclave was chilled to room temperature, and the white precipitate was filtered and washed with distilled water/absolute ethanol solution. The product was dried in an oven at 100 °C for 12 h to collect ZnO nanoneedles.

Fig. 1 a The experimental setup diagram of the synthesized ZnO nanoneedles via hydrothermal method and its coating on the substrate. **b** The schematic block diagram of our handmade gas sensing setup

2.2.2 Sensor preparation

1 gr of polyvinyl alcohol was added into 99 mL of deionized water and heated at 90 °C to obtain a transparent polyvinyl alcohol solution of 1 wt%. 1 gr of ZnO powder was added to 17 ml of deionized water, stirred and ultrasonicated to achieve a milky solution. The prepared solution was added into the 3 ml of 1 wt% polyvinyl alcohol solution and then was stirred to obtain a solution containing ZnO nanostructures [solution (c)]. An epoxy glass substrate with a 2×2 cm^2 area of the finger type Cu-interdigitated electrodes was used for sensor preparation. The width of overlap electrodes and the gap between two successive electrodes was 0.4 mm. Before use, the epoxy glass substrate was cleaned by ultrasonic treatment in acetone and hot soap-water solution, then rinsed thoroughly with deionized water and dried under relative vacuum. The solution (c) was deposited on the substrate using the spin coating instrument (Nano Ebtekar Paidar Co., Iran) under a speed of 500 rpm. The deposited

layer was dried in an oven at 100 °C, to remove polyvinyl alcohol in the coated layer and this prepared sensor was used as the CO gas sensor. Figure 1b shows the schematic diagram of our handmade gas sensor setup that used for the test of the sensor.

2.2.3 Characterization

A Philips-PW 1730 X-ray diffractometer (Philips, Eindhoven, The Netherlands) with copper radiation (Cu–Ka, $\lambda = 1.54$ Å) and a working voltage of 30 kV, was used for X-ray diffractometry (XRD) analysis. The step-scanning measurements of the instrument were 10–80° 2θ, with a step of 0.04 2θ and a counting time of 4 s per step. The surface morphology of the deposited sample was studied by a field effect scanning electron microscopy (FESEM-TESCAN-MRIA3, The Czech Republic) at 30 kV, equipped with an energy dispersive X-ray spectroscopy (EDX) detector. The specific surface area of the prepared sample was analyzed and measured with a BELSORP-MR6, Microtrac BEL Japan Inc. spectroscopy, using Brunauer–Emmett–Teller (BET) theory.

3 Results and discussion

3.1 ZnO characterization

The XRD pattern of the ZnO sample is plotted in Fig. 2a. According to this figure, there are a series of diffraction peaks at 2θ = 31.72°, 34.35°, 36.19°, 47.46°, 56.56°, 62.78°, 67.9° corresponding to Miller indices of (100), (002), (101), (102), (110), (103), (112) of ZnO crystal structure (JCPDS Card No. 01-076-0704) [5, 8, 9, 18]. These diffraction peaks present hexagonal wurtzite phase of the pure crystallized ZnO without other impurities [9, 18]. The crystalline grain size (D) of the sample was determined using the Debye–Scherrer's relation [5]:

$$D = \frac{K\lambda}{\beta_{hkl} \cos\theta_{hkl}} \tag{1}$$

where, D is the crystalline grain size, K is the shape factor, $\lambda = 1.54$ Å is the X-ray wavelength, θ_{hkl} is the diffraction angle, and β_{hkl} is the full width at half maximum intensity (in radians). The crystalline particle size of ZnO nanoneedles is found to be 40 nm.

Figure 2b and c display the FESEM images of the ZnO sensor surface with different magnification. According to the FESEM images, the synthesized ZnO has uniform thin needle morphology. Moreover, the synthesized ZnO nanoneedles (ZONs) possess sharp tips and wider bases with high porosity and dispersed distribution (see Fig. 2b, c). The average lengths and diameters of the nanoneedles are ~ 3–5 μm

and ~ 100–200 nm, respectively. Figure 2d shows the EDX spectra of the sample. The calculated atomic percentage is tabulated in the table of the figure. As can be seen in Fig. 2d, the present peaks relative to Zinc and oxygen ions which indicate the purity of the synthesized ZONs.

Figure 2e displays a BET analysis of the ZON sample through nitrogen adsorption–desorption measurements, which is important to get extra information about the inner architectures of the sensor surface. The isotherm curve of ZONs in Fig. 2e with a hysteresis loop at the P/P_o range of 0.3–0.9, illustrates the existence of mesopores in range of 5–50 nm [23, 25]. The adsorbed nitrogen value increased very precipitously at P/P_o > 0.8, which suggests the existence of macropores (> 50 nm in diameter) in the ZON [26–28]. Figure 2f displays the curve of V_a versus the pore size distribution for the sample. The specific surface area of ZON is 31.7 $m^2 \cdot g^{-1}$ and the average pore size is about 4–8 nm, which is calculated by using the BJH method.

3.2 CO sensing behavior of the sensor

The ZON sensor film (ZS) response is defined as the resistance change ratio of the device under pure air and test gas atmosphere, which is given by the equation [4, 5]:

$$\text{Response}(\%) = \left[\frac{R_{air} - R_{gas}}{R_{air}}\right] \times 100 \tag{2}$$

where R_{air} and R_{gas} are the resistance of sensor in pure air and gas atmosphere, respectively. Two important sensing parameters of the response time and recovery time are defined as the time required to reach 90% of the final resistance change, when the gas is turned on and off, respectively [4, 5].

It is well known that the response of SMO sensors such as ZS at environmental conditions is highly influenced by relative humidity (RH) [1, 2, 24]. Therefore, to begin with, CO is used as the probe gas to perform gas-sensing tests at varying RH to examine RH. Figure 3a shows the dynamic resistance changes of the ZS under different CO concentrations at various RH and it has a baseline resistance of about 40.95, 39.8, 38.9 and 38.1 MΩ at different RHs of 30%, 50%, 70%, and 90%, respectively. This reduction of sensor baseline resistance with increasing humidity is due to that dual surface hydroxyls per water molecule can be formed on the ZS surface by the chemisorption of water molecules and the carrier hopping mechanism is possible to charge transport in this added layer [29]. Moreover, through the increasing RH level, the active sites on the ZS surface are occupied by more water molecules, and extra water molecules can form an additional layer on the initial chemisorption water layer following the physisorption process [1, 29]. Hence, the free movement of the protons along the physisorption
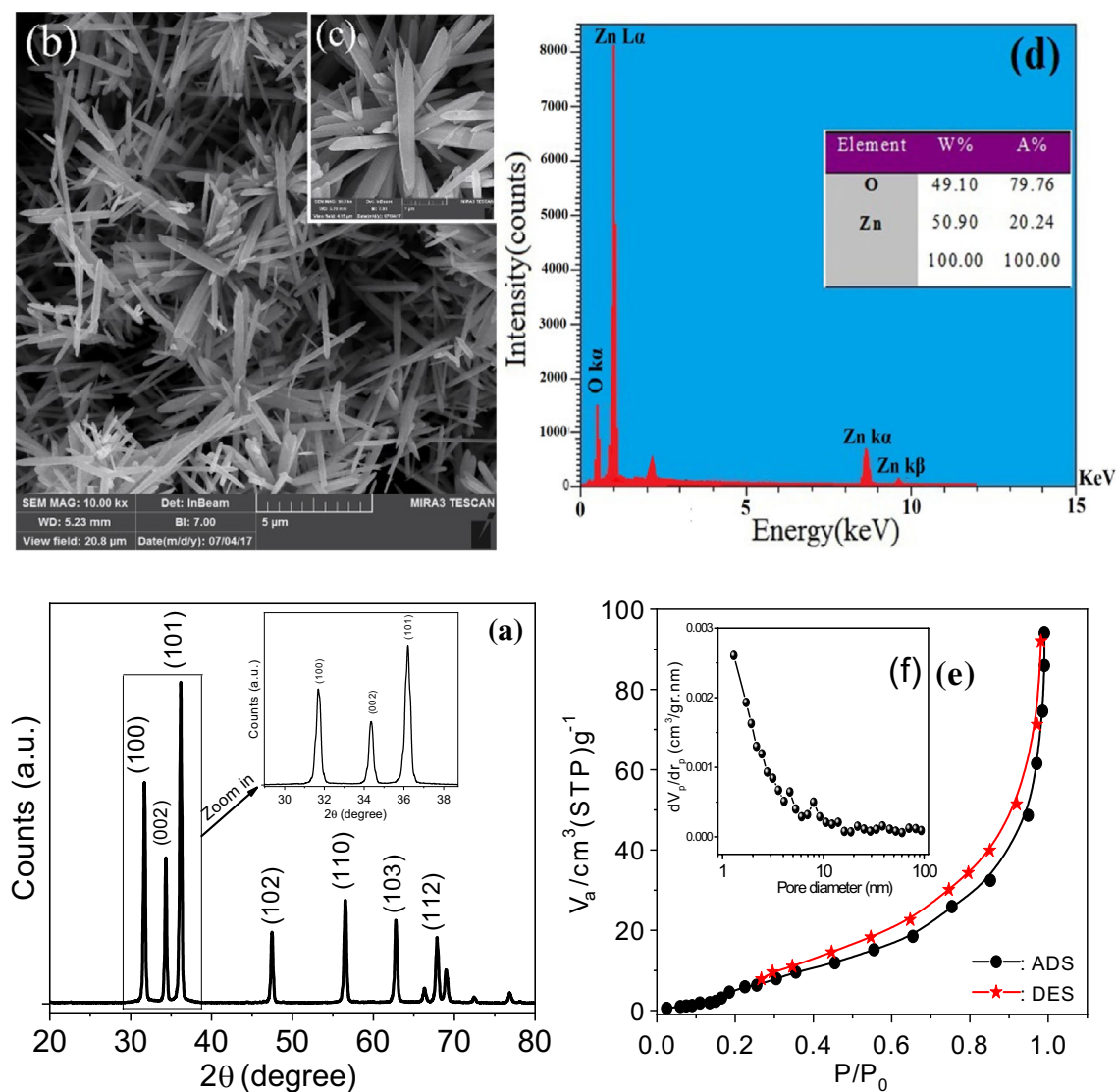
Fig. 2 **a** XRD pattern, **b**, **c** FESEM images with different magnification and **d** EDX pattern of the prepared sample. **e** N$_2$ absorption–desorption isotherms of the ZONs and the inset image **f** is the pore-size distribution calculated by BJH method from the desorption curves
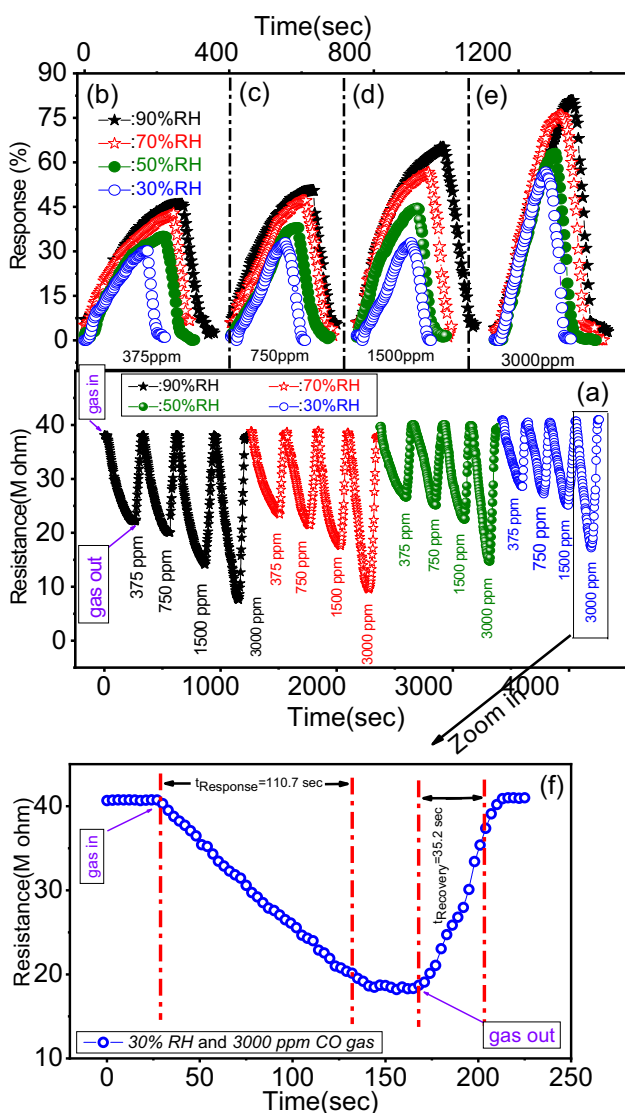
water layer causes the ZS baseline resistance decreases with increasing RH.

According to Fig. 3a results, under gas injection condition, the resistance of the ZS decreased, and it reached a steady state within a few seconds. In spite of the fact that the resistance change value of the ZS increased with the increasing gas concentration in each RH, it slightly decreased with an RH reduction in each gas concentration. The reason for the resistance change with decreasing RH is mainly due to the change of the number of sensor surface active sites for adsorption and desorption of gas molecules. The highest (lowest) resistance change of 32.9 MΩ (10.4 MΩ) belonged to 3000 (375) ppm gas at 90% (30%) RH. After that the sensor reached the steady state point at certain CO gas concentration and RH, the pure air was introduced into the

test chamber, and the sensor resistance value was found to increase rapidly, so that it reached the initial baseline resistance value after a few time.

The response and recovery behaviors are two significant features for evaluating the performance of the gas sensors. According to the results of Fig. 3a, the dependence of the ZS response to humidity toward different CO concentrations was shown in Fig. 3b–e and the response, response time and recovery time noted in Table 1. According to Fig. 3b–e results, the response of the ZS is increased in each RH with increasing gas concentration, while the CO gas response of the device is decreased in each gas concentration with decreasing RH. The rise of the sensor response with the increasing gas concentration in each RH is for the reason that the penetration and interaction of sufficient gas molecules

Fig. 3 **a** The dynamic changes of the resistance versus time in the ZS, under different RH and various CO gas concentrations. **b–e** The response versus time curves of the ZS toward different gas concentrations at room temperature and various RH. **f** The dynamic change of the resistance versus time toward 3000 ppm CO in 30% RH. The lines are a guide for eyes

Table 1 The response, response time and recovery time of ZS toward different CO concentrations at room temperature and various RH

Gas concentrations (ppm)	RH (%)	Response (%)	$t_{response}$ (sec)	$t_{recovery}$ (sec)
375	90	45.9	233.3	43.2
	70	41.9	202.5	40.5
	50	33.6	186.3	37.8
	30	29.7	161.4	29.7
750	90	52.5	218.7	54
	70	47.1	180.9	51.3
	50	37.9	172.8	43.2
	30	32.9	151.2	33.7
1500	90	65	207	67.5
	70	56.5	159	45.9
	50	46.5	148.4	40.7
	30	39.8	135.3	34.1
3000	90	80.8	186.3	75.6
	70	75.1	118.8	64
	50	63.9	113.3	47.8
	30	56.7	110.7	35.2

and the gas concentration with a positive slope was observed in each RH, fitted to $y = ax + b$ with an acceptable regression analysis. Figure 4a shows the ZS response increased with the increasing gas concentration in each RH. Moreover, Fig. 4a exposes that a decrease of RH from 90% to 30%, causes the response of the ZS to drop under different gas concentrations. Also, the plotted sensor response versus the gas concentration at 90% (30%) RH, has the highest (lowest) slope, which it is due to the direct effect of water molecules on active surface sites of the sensor at high RH.

The response/recovery time calculated from Fig. 3a–e and noted in Table 1. Accordingly, the lowest response time (recovery time) of 140.4 s (29.7 s) at 375 ppm CO gas concentration and under 30% RH, was obtained. Figure 4b shows the plots of the ZS response versus RH at various gas concentrations which they have the positive linear slope with high accuracy. Herein, a significant increase in the response is observed with increasing RH and also CO concentration. The enhancement of the response in high CO concentration is probably due to that an additional interaction between the gas molecules and the active sites of the sensor surface occur so that the lowest (highest) ZS response created in 375 ppm (3000 ppm) gas concentration. Moreover the increase of the ZS response with increasing RH in certain gas concentration is due to the extra hydroxyl active sites creation on the sensor surface and the increase of the conductivity. The ZS response toward 375 ppm gas was 45.9% in 90% RH, and it changed to 29.7% in 30% RH, which has a change of about 35%. This change of the response toward 750, 1500 and 3000 ppm gas concentration was 37%, 38% and 31% from 90
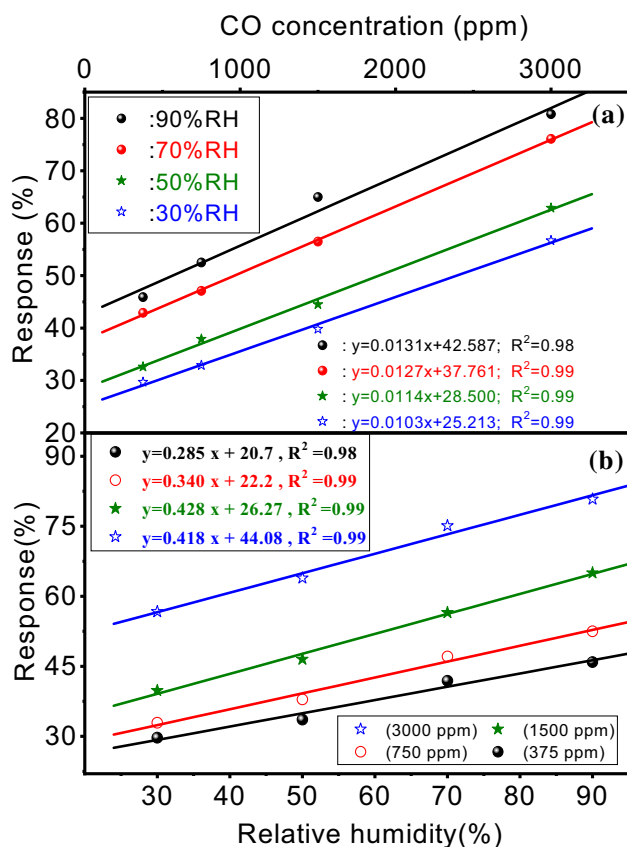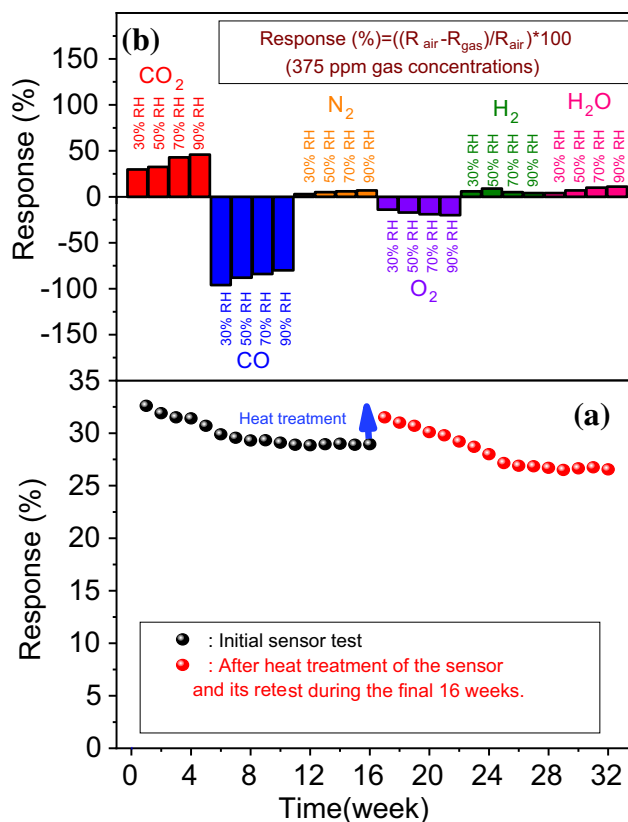
with the surface components of the sensor are enhanced. Moreover, it seems that the ZS response depends on RH levels because the response increased with the increasing RH in each CO gas concentration. The reason for this phenomenon is probably that, the further hydroxyl active sites on the sensor surface at high RH, could be causing more significant reactions between the gas molecules and the sensor surface occur, so that the highest (lowest) ZS response of 80.8% (29.7%) belonged to 3000 (375) ppm gas at 90% (30%) RH. According to the results of Fig. 3a–e and Table 1, the sensor response versus the gas concentration at each RH was plotted in Fig. 4a. A linear relationship between the response

Fig. 4 **a** The ZS response versus different CO concentrations ranging from 375 to 3000 ppm at various RHs and room temperature. **b** The device response versus RH ranging from 30% to 90% toward various gas concentrations at room temperature. The fitting lines obtained by the linear regression and plotted in curves

Fig. 5 **a** The response changes of the ZS in initial test during a period of 16 weeks and during same time after heat treatment by oven drying at 100 °C for the half day. **b** The response selectivity of the ZS toward 375 ppm of various gases at room temperature and different RHs

RH to 30% RH. Therefore, the RH is the main factor on the ZS for CO detection, so that with decreasing RH from 90 to 30%, the sensor response changed about 31–38%. In spite of the fact that the sensor response has been changed in different RH, the ZS had a measurable CO response even in 30% RH and various gas concentrations. As a result, the linear relationship between the response and the CO concentration and also RH are decisive factors for the practical use of the ZS under various RH at room temperature.

Long-term stability of a gas sensor is an important parameter from the viewpoint of practical applications. Figure 5a illustrates the long-term stability of the ZS during 16 weeks toward 375 ppm CO gas at room temperature. It can be seen from Fig. 5a that the ZS displays measurable stability after 16 weeks with a small response degradation of 9%. The stability and repeatability have been examined by applying ZS to sequential gas sensing tests throughout 1 week at room temperature. As shown in Fig. 5a, the sensor reached the same steady state after 8 weeks, and it kept it between 9 and 16 weeks. After 16 weeks and to examine the sensor

reversibility, the sensor was heated by oven drying at 100 °C for the half day. After heat treatment of the sensor, its test toward 375 ppm CO gas was resumed under in initial test condition and up to 32 weeks, which the results are plotted in Fig. 5a. A 14% response reduction was observed between 17 and 25 weeks. Moreover, the sensor reached the same steady state between 26 and 32 weeks, but it takes place lower response than that the same period of the initial test.

From a practical point of view, the selectivity of a sensor is a significant parameter, because a sensor displays some degree of response to all tested gases which results in limited applications. Moreover, CO gas is an atmospheric gas pollutant which is generally created through incomplete combustion of wood, crude oil and natural gas derivatives with other pollutants such as CO_2, therefore the CO detection ability between other air components is an important factor for a CO sensor. To examine of the ZS selectivity, it was exposed to 375 ppm of the various gases such as CO_2, N_2, O_2, H_2 and H_2O at room operating temperature, which the response results have been shown in Fig. 5b. It can be seen that the sensing behavior of the ZS for

various gases is different so that the sensor did not show a meaningful response to N_2, O_2, H_2 and H_2O, while its response to CO and CO_2 was strong. Moreover, the largest CO response of the ZS demonstrates that it has a good ability for CO detection between different tested gases. The CO sensing results of the ZS have been compared with the previous works in Refs. [5–9, 18, 19, 24, 30], and the detailed comparison is shown in Table 2. Accordingly, other reported CO sensors in Refs. [5–9, 18, 19] have the sensitivity to low gas concentration, but they have high operating temperature and response time with a low response. Moreover, the comparison of the present work results with Refs. [24, 30], shows our handmade sensor has not only good response and suitable response time than that previous reports but also long-term stability (see Fig. 5a) and CO gas selectivity (Fig. 5b) at room temperature and various RHs.
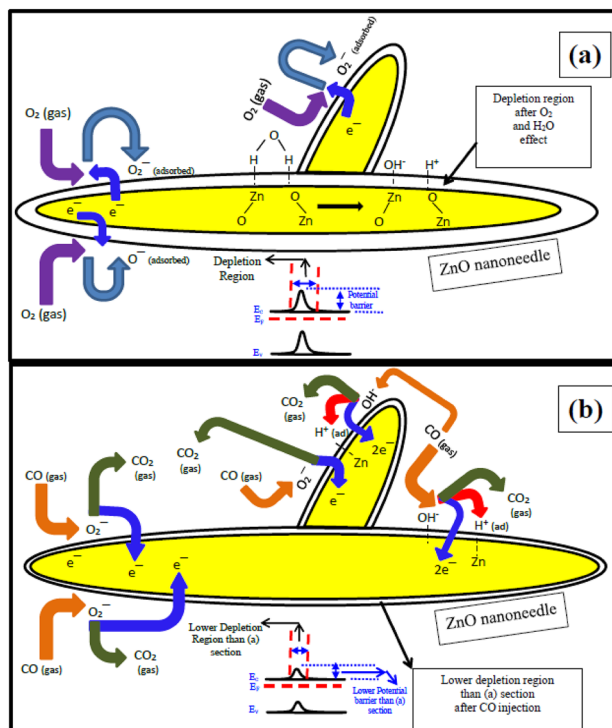
3.3 Gas sensing mechanism of ZS

The adsorption and desorption of CO molecules on the surface components of the ZS such as lattice ions, oxygen species or water molecules; with the charge redistribution between them are fundamental to the sensor performance.

Oxygen as an oxidizing gas tends to interaction and absorption on the ZS surface at low operating temperatures (< 100 °C) [1, 29]. These adsorbed oxygen molecules captured electrons from the conduction band of the ZnO to produce negatively charged oxygen ions, as shown in Eqs. 3–5 [1, 6, 31] and Fig. 6a:

$$O_2(gas) \leftrightarrow O_2(adsorbed) \tag{3}$$

$$O_2(adsorbed) + e^- \rightarrow O_2^- \tag{4}$$

$$O_2(adsorbed) + 2e^- \rightarrow 2O^- \tag{5}$$

The trapped electrons through above mechanism cause an increase in not only the width of charge depletion region (the

Fig. 6 The schematic diagram for **a** the adsorbed oxygen and water molecules on the sensor surface at ambient conditions, and **b** CO sensing mechanism of the ZS at room temperature

space charge region) but also the potential barrier height between the grains of the sensor surface, occurs.
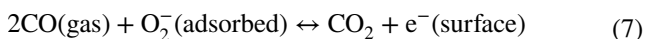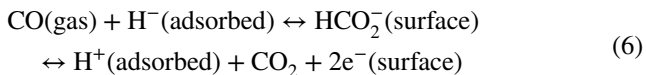
In this condition, with increasing RH, the water molecules interact with "two metal oxides" or "a metal oxide and a surface oxygen ion" which the result is "two Zn–OH dipoles" or "Zn–OH and O^-–$H^{+"}$", respectively, as shown in Fig. 6a. These results lead to not only the formation of the hydroxyl ions on the sensor surface but also the return of the

Table 2 Comparison of the CO-sensing characteristics of some sensors based on ZnO which reported in previous literatures with the prepared ZS in the present work

Used material	Response (%)	Response time	Recovery time	Gas concentration (ppm)	Operating temperature (°C)	Ref.
Al–ZnO	80	≥ 3 min	≥ 3 min	50	300	[5]
ZnO	81.2	180 s	210 s	30	300	[6]
In–ZnO	5	20 s	45 s	50	300	[7]
ZnO	22	≥ 10 min	≥ 5 min	200	300	[8]
ZnO	14	–	–	9000	400	[9]
ZnO nanoroad	30	–	–	10	350	[18]
Pd–ZnO	6.592	≥ 100 s	≥ 500 s	1000	300	[19]
ZnO	14	≥ 5 min	≥ 4 min	250	Room temperature	[24]
Au–SnO2–ZnO	1.62	≥ 400 s	≥ 50 s	50	Room temperature	[31]
ZnO nanoneedles	33.6	186.3	37.8	375	Room temperature	This work
ZnO nanoneedles	63.9	113.3	47.8	3000	Room temperature	His work

surface trapped electrons into the conduction band of ZS. Accordingly, the conductivity of the ZS surface should be increased with the increase of the water molecules, which is corresponded with the results of Fig. 3a.

After gas injection, the CO molecules as reducing agents act with ZS surface components and the result is an increase of the electrons concentration on the sensor surface. In low RH ($\approx 30\%$) and room temperature, CO reacts with not only chemisorbed oxygen ions (O_2^-), but also the surface hydroxyls to form carbon dioxide; as given in Eqs. 6, 7 [1, 2, 16, 23, 30]:

$$CO(gas) + H^-(adsorbed) \leftrightarrow HCO_2^-(surface)$$
$$\leftrightarrow H^+(adsorbed) + CO_2 + 2e^-(surface) \quad (6)$$

$$2CO(gas) + O_2^-(adsorbed) \leftrightarrow CO_2 + e^-(surface) \quad (7)$$

These interactions led to that the surface trapped electrons will be released back to the conduction band of ZS (see Fig. 6b). Moreover, the released electrons cause not only the depletion region at the nanoneedles interface will shrink, but also the barrier height will decrease. The result is the decrease of the sensor resistance at CO atmosphere (see Fig. 3a). On the other hand, an increase of RH during CO injection could enhance the surface hydroxyls and hydrogen ions, which leads to more surface reaction sites of the ZS than the wet atmosphere. Under this condition, the ZS surface has a tendency for the formation of formate (HCO_2^-) ions, which is an intermediate product in the interaction of CO molecules with ZS surface [1, 29]. Subsequently, the interaction between HCO_2^- ions and the surface hydrogen ions causes the greater surface trapped electrons will be released back to the conduction band of ZS. The result is the more decrease (increase) of the ZS sensor resistance (response) through increasing RH (see Figs. 5 and 6b). Furthermore, the increase of the sensor response with the increase of the gas concentrations (see Fig. 5) is for the reason that the penetration and the interaction of sufficient gas molecules and the surface components of the sensor increase with the increasing gas concentrations.

4 Conclusion

In the present work, 1D-nanoneedles of ZnO were synthesized by a simple hydrothermal method and used for CO detection. XRD, FESEM, EDX and BET analysis confirmed the formation of the crystal structure of 1D-nanoneedles ZnO in hexagonal wurtzite phase with good porosity. The CO gas sensing features of ZS were carefully investigated toward various CO concentrations at ambient conditions. Moreover, the sensor response and selectivity were examined

for different gases. The humidity effect as an important parameter for CO gas sensing of ZS resistance-type at room temperature and air pressure was evaluated. The CO sensing results demonstrated that the optimal sensor response at room temperature is depended to gas concentrations and RHs of the test conditions so that the highest (lowest) ZS response of 80.8% (29.7%) belonged to 3000 (375) ppm gas at 90% (30%) RH. Moreover, the response, resistance change, response time and recovery time decreased with decreasing RH at different CO gas concentrations and room temperature, so that the sensor response had a change of 31–38% when the RH changed from 90 to 30%. Finally, the use of heat treatment after 4 months was a new and practical method for the response recovery of the ZS which facilitates its use for inaccessible areas.

References

1. P. Shankar, J. Rayappan, Gas sensing mechanism of metal oxides: the role of ambient atmosphere, type of semiconductor and gases. Sci. Lett. J. **4**(126), 1–18 (2015)
2. L. Zhu, W. Zeng, Room-temperature gas sensing of ZnO-based gas sensor: a review. Sens. Actuat. A **267**, 242–261 (2017)
3. L. Wang, R. Chai, Z. Lou, G. Shen, Highly sensitive hybrid nanofiber-based room-temperature CO sensors: experiments and density functional theory Simulations. Nano Res. **11**(2), 1029–1037 (2018)
4. L. Hou, C. Zhang, L. Li, C. Du, X. Li, X. Kang, W. Chen, CO gas sensors based on p-type CuO nanotubes and CuO nanocubes: morphology and surface structure effects on the sensing performance. Talanta **188**, 41–49 (2018)
5. F. Liang, S. Chen, W. Xie, C. Zou, The decoration of Nb-doped TiO_2 microspheres by reduced graphene oxide for enhanced CO gas sensing. J. Phys. Chem. Solids **114**, 195–200 (2018)
6. C.S. Prajapati, D. Visser, S. Anand, N. Bhat, Honeycomb type ZnO nanostructures for sensitive and selective CO detection. Sens. Actuat. B **252**, 764–772 (2017)
7. R. Dhahri, M. Hjiri, L. El Mir, H. Alamri, A. Bonavita, D. Iannazzo, S.G. Leonardi, G. Ner, CO sensing characteristics of In-doped ZnO semiconductor nanoparticles. J. Sci. Adv. Mater. Devices **2**(1), 34–40 (2017)
8. M. Dwivedi, J. Bhargava, A. Sharma, V. Vyas, G. Eranna, CO sensor using ZnO thin film derived by RF magnetron sputtering technique. IEEE Sens. J. **14**(5), 1577–1582 (2014)
9. N. Han, H. Liu, X. Wu, D. Li, L. Chai, Y. Chen, Pure and Sn-, Ga- and Mn-doped ZnO gas sensors working at different temperatures for formaldehyde, humidity, NH_3, toluene and CO. Appl. Phys. A **104**, 627–633 (2011)
10. F. Juang, W. Chern, B. Chen, Carbon dioxide gas sensing properties of ZnSn(OH)_6-ZnO nanocomposites with ZnO nanorod structures. Thin Solid Films **660**, 771–776 (2018)
11. N.H. Ha, D.D. Thinh, N.T. Huong, N.H. Phuong, P.D. Thach, H.S. Hong, Fast response of carbon monoxide gas sensors using a highly porous network of ZnO nanoparticles decorated on 3D reduced grapheme oxide. Appl. Surf. Sci. **434**, 1048–1054 (2018)
12. J. Wang, J. Yang, N. Han, X. Zhou, S. Gong, J. Yang, P. Hu, Y. Chen, Highly sensitive and selective ethanol and acetone gas sensors based on modified ZnO nanomaterials. Mater. Design. **121**, 69–76 (2017)

13. J. Zhang, S. Wang, Y. Wang, M. Xu, H. Xia, S. Zhang, W. Huang, X. Guo, S. Wu, ZnO hollow spheres: preparation, characterization, and gas sensing properties. Sens. Actuat. B **139**, 411–417 (2009)

14. V.M. Latyshev, T.O. Berestok, A.S. Opanasyuk, A.S. Kornyushchenko, V.I. Perekrestov, Nanostructured ZnO films for potential use in LPG gas sensors. Solid State Sci. **67**, 109–113 (2017)

15. C.H. Tan, S.T. Tan, H.B. Lee, R.T. Ginting, H.F. Oleiwi, C.C. Yap, M.H. HajiJumali, M. Yahaya, Automated room temperature optical absorbance CO sensor based on in-doped ZnO nanorod. Sens. Actuat. B **248**, 140–152 (2017)

16. J. Kim, A. Mirzaei, H. Kim, S. Kim, Extremely sensitive and selective sub-ppm CO detection by thesynergistic effect of Au nanoparticles and core–shell nanowires. Sens. Actuat. B **249**, 177–188 (2017)

17. A. Mirzaei, S. Park, G. Sun, H. Kheel, C. Lee, CO gas sensing properties of $In_4Sn_3O_{12}$ and TeO_2 compositenanoparticle sensors. J. Hazard. Mater. **305**, 130–138 (2016)

18. S. Zhang, J. Lim, J. Huh, W. Lee, Selective growth of ZnO nanorods and its gas sensor application. IEEE Sens. J. **12**(11), 3143–3148 (2012)

19. W. Moon, Y. Jun, H. Kim, W. Kim, S. Hong, CO gas sensing properties in Pd-added ZnO sensors. J. Electroceram. **23**, 196–199 (2009)

20. D. Zhang, Y. Sun, C. Jiang, Y. Yao, D. Wang, Y. Zhang, Room-temperature highly sensitive CO gas sensor based on Ag-loaded zinc oxide/molybdenum disulfide ternary nanocomposite and its sensing properties. Sens. Actuat. B **253**, 1120–1128 (2017)

21. M. Hjiri, R. Dhahri, L. El Mir, S.G. Leonardi, G. Neri, Excellent CO gas sensor based on Ga-doped ZnO nanoparticles. J. Mater. Sci. **26**(8), 6020–6024 (2015)

22. M. Hjiri, L. El Mir, S.G. Leonardi, A. Pistone, L. Mavilia, G. Neri, Al-doped ZnO for highly sensitive CO gas sensors. Sens. Actuat. B **196**, 413–420 (2014)

23. C.R. Michel, A.H. Martínez-Preciado, R. Parra, C.M. Aldao, M.A. Ponce, Novel CO_2 and CO gas sensor based on nanostructured Sm_2O_3 hollow microspheres. Sens. Actuat. B **202**, 1220–1228 (2014)

24. H. Zhang, Y. Long, Z. Li, B. Sun, Fabrication of comb-like ZnO nanostructures for room-temperature CO gas sensing application. Vacuum **101**, 113–117 (2014)

25. F. Arabloo, S. Javadpour, R. Memarzadeh, F. Panahi, M.D. Emami, M.H. Shariat, The interaction of carbon monoxide to Fe(III)(salen)-PEDOT:PSS composite as a gas sensor. Synth. Met. **209**, 192–199 (2015)

26. T. Hojati, M. Ebrahimi, R. Afzalzadeh, Highly sensitive CO sensor based on ZnO/MWCNT nano sheet network grown via hydrothermal method. Mater. Chem. Phys. **207**, 50–57 (2018)

27. X. Xing, X. Xiao, L. Wang, Y. Wang, Highly sensitive formaldehyde gas sensor based on hierarchically porous Ag- loaded ZnO heterojunction nanocomposites. Sens. Actuat. B **247**, 797–806 (2017)

28. T.Y. Ma, X.J. Zhang, Z.Y. Yuan, Hierarchical meso-/macroporous aluminum phosphonate hybrid materials as multifunctional adsorbents. J. Phys. Chem. C **113**, 12854–12862 (2009)

29. P. Kannan, R. Sarawathi, J. Rayappan, A highly sensitive humidity sensor based on DC reactive magnetron sputterd zink oxide thin film. Sens. Actuat. A **164**, 8–14 (2010)

30. J. Kim, A. Mirzaei, H.W. Kim, S.S. Kim, Low power-consumption CO gas sensors based on Au-functionalized SnO_2-ZnO core-shell nanowires. Sens. Actuat. B **267**, 597–607 (2018)

31. M. Singh, B. Yadav, A. Ranjan, M. Kaur, S. Gupta, Synthesis and characterization of perovskite barium titanate thin film and its application as LPG sensor. Sens. Actuat. B **241**, 1170–1178 (2017)